J Mol Model (2013) 19:5113–5127
DOI 10.1007/s00894-013-1980-z

ORIGINAL PAPER

Structure and spectral characteristics of diquat-cucurbituril complexes from density functional theory

Swarada R. Peerannawar · Shridhar P. Gejji

Received: 23 May 2013 / Accepted: 21 August 2013 / Published online: 3 October 2013

Abstract Electronic structure, ^{1}H NMR and infrared spectra of diquat (6,7-dihydrodipyrido[1,2-b:1′,2′-e] pyrazine-5,8-diium or DQ^{2+}) encapsulated by cucurbit[n]uril (n = 7,8) hosts are obtained using the density functional theory. Theoretical calculations have shown that both CB[7] or CB[8] host possesses strong affinity toward DQ^{2+} compared to its reduced cation or neutral species. Calculated ^{1}H NMR spectra reveal that H_α protons on bi-pyridinium rings of DQ^{2+}@CB[8] complex are de-shielded owing to C=O···H interactions. On the other hand aromatic (H_β and H_δ) of DQ^{2+} within the CB[8] cavity exhibit significant shielding. The complexation of CB[8] with DQ^{2+} splits the carbonyl stretching vibration (1788 cm^{-1}) into two distinct vibrations which correspond to 1765 cm^{-1} arising from hydrogen bonded carbonyls and the 1792 cm^{-1} band from non-interacting ones. Further, the CN stretching vibration in DQ^{2+} exhibits a frequency blue-shift of 6 cm^{-1} on its encapsulation within the CB[8] cavity. The direction of frequency shift has been explained on the basis of natural bond orbital analyses.

Keywords Cucurbit[8]uril · Density functional theory · ^{1}H NMR · Normal vibrations · Viologen

Introduction

Viologens exhibit two distinct forms viz., paraquat (1,1′-Dimethyl-4,4′-bipyridinium) and diquat (6,7-dihydrodipyrido[1,2-b:1′,2′-e] pyrazine-5,8-diium) and are biologically important owing to their interesting physicochemical properties [1]. The viologen guests find applications as redox couples [2] and are further explored in electro-chromic materials [3], electro-catalysis, solar energy conversion, molecular electronics [4] and supramolecular host–guest chemistry [5]. Viologens with their strong reducing ability exhibit different oxidation states. It has been observed that DQ^+ act as electric conductor interrupting natural electron transfer chain in biological systems. Moreover, electrochemical properties of viologen encapsulated by supramolecular hosts such as cyclodextrin, cucurbituril, calixarene etc. are studied in the literature [5–7]. In particular, it has been observed that cucurbituril hosts endowed with characteristic barrel shape cavity and carbonyl laced portals can accommodate a variety of guest molecules to conduce kinetically stable inclusion complexes with viologens or their derivatives. Electron transfer reactions in cucurbituril host encapsulated with redox active guest has been a subject of growing interest. Kaifer and his coworkers have carried out experimental investigations on inclusion complexes of redox active diquat (DQ^{2+}) and paraquat (PQ^{2+}) ion confined within cavity of cucurbituril hosts using the X-ray diffraction, ^{1}H NMR, UV/Vis, fluorescence spectroscopy and mass spectrometry experiments [8] and demonstrated their binding selectivity toward viologens. Both paraquat and diquat forms of viologen reveal stronger binding affinity toward CB[8]. It has further been concluded that reduction of di-cationic viologen within the host-cavity facilitated through a two step mechanism which yields cation and neutral species. Consequently Kim et al. [9] have carried out detailed experimental investigations on one electron reduction of PQ^{2+} accompanying the formation of dimer within the cavity of CB[8].

In spite of all these experimental studies on viologen guests confined within CB[n] macrocycle, attempts to gain deeper insights for inclusion of DQ^{2+} inside the host cavity are scanty. On

Electronic supplementary material The online version of this article (doi:10.1007/s00894-013-1980-z) contains supplementary material, which is available to authorized users.

S. R. Peerannawar · S. P. Gejji (✉)
Department of Chemistry, University of Pune, Pune 411 007, India
e-mail: spgejji@chem.unipune.ac.in

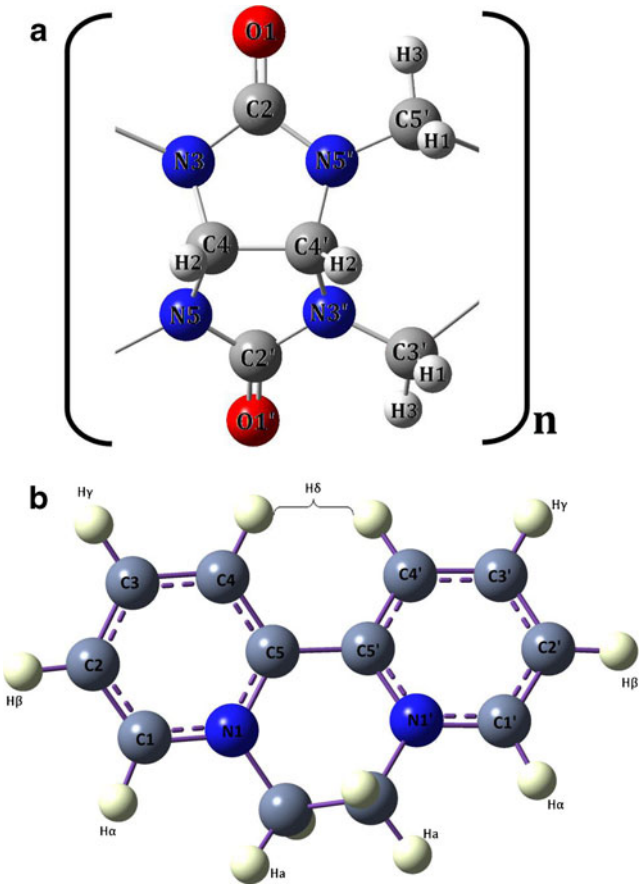

Fig. 1 **a** Cucurbituril monomer **b** Diquat guest along with numbering scheme. The *blue* and *red* atoms denote nitrogen and oxygen centers

theoretical front, molecular dynamics simulations on paraquat (PQ^{2+}) complexed with CB[*n*] (*n* =6–8) hosts [10] suggested that PQ^{2+} penetrates deeper within the host cavity. It has also been inferred that electrostatic interactions contribute largely to the host–guest binding along with the dipole–dipole interactions which show a strong dependence on the separation of N–N atoms in viologen di-cations. The present work focuses on deriving the electronic structure, ^{1}H NMR and vibrational characteristics of DQ^{2+} encapsulated CB[n] hosts using the density functional theory. The ^{1}H NMR of individual hosts, their viologen complexes along with one electron reduction products viz., cation and neutral forms thereof are obtained. We analyze how hydrogen bonding interactions conduce complexation of DQ^{2+} with CB[n] (*n* =7, 8) and further how such interactions reflect in characteristic vibrational frequencies. The computational method is outlined below.

Computational methods

The individual CB[7] and CB[8] hosts, DQ^{2+} guest and their inclusion complexes were optimized within the framework of density functional theory incorporating the 6-31G(d,p) basis set. The GAUSSIAN-09 program was employed [11]. Structural parameters and ^{1}H NMR chemical shifts from the density functional calculations employing a variety of functionals which include (a) Becke's three-parameter [12] exchange combined with Lee, Yang and Parr correlation functional (B3LYP) [13] (b) Grimme's B97D functional [14] which is widely used to describe dispersive interactions and lastly (c) hybrid functional due to Perdew, Burke and Ernzerh (PBE0) [15–17] that accounts for weak non covalent interactions. Basis set superposition error (BSSE) was estimated for each complex.

Different host–guest complexes with either partial or complete encapsulation of DQ^{2+} were considered. The products of two step electron reduction of the lowest energy complex were subsequently analyzed at the same level of theory. Optimized structures of host–guest complexes were confirmed to be local minima from vibrational frequency calculations (all the vibrational frequencies turn out to be real for these structures). Normal vibrations were assigned by visualizing the displacement of

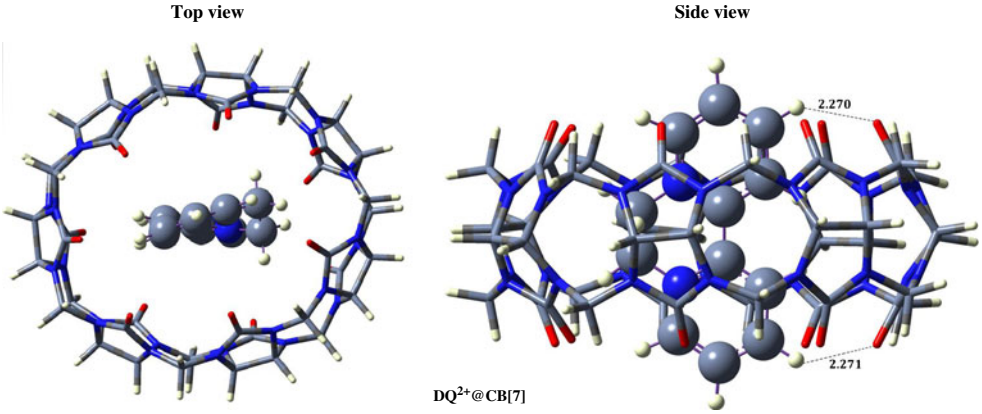

Fig. 2 B3LYP/6-31G(d,p) gas phase optimized geometry of DQ^{2+}@CB[7]

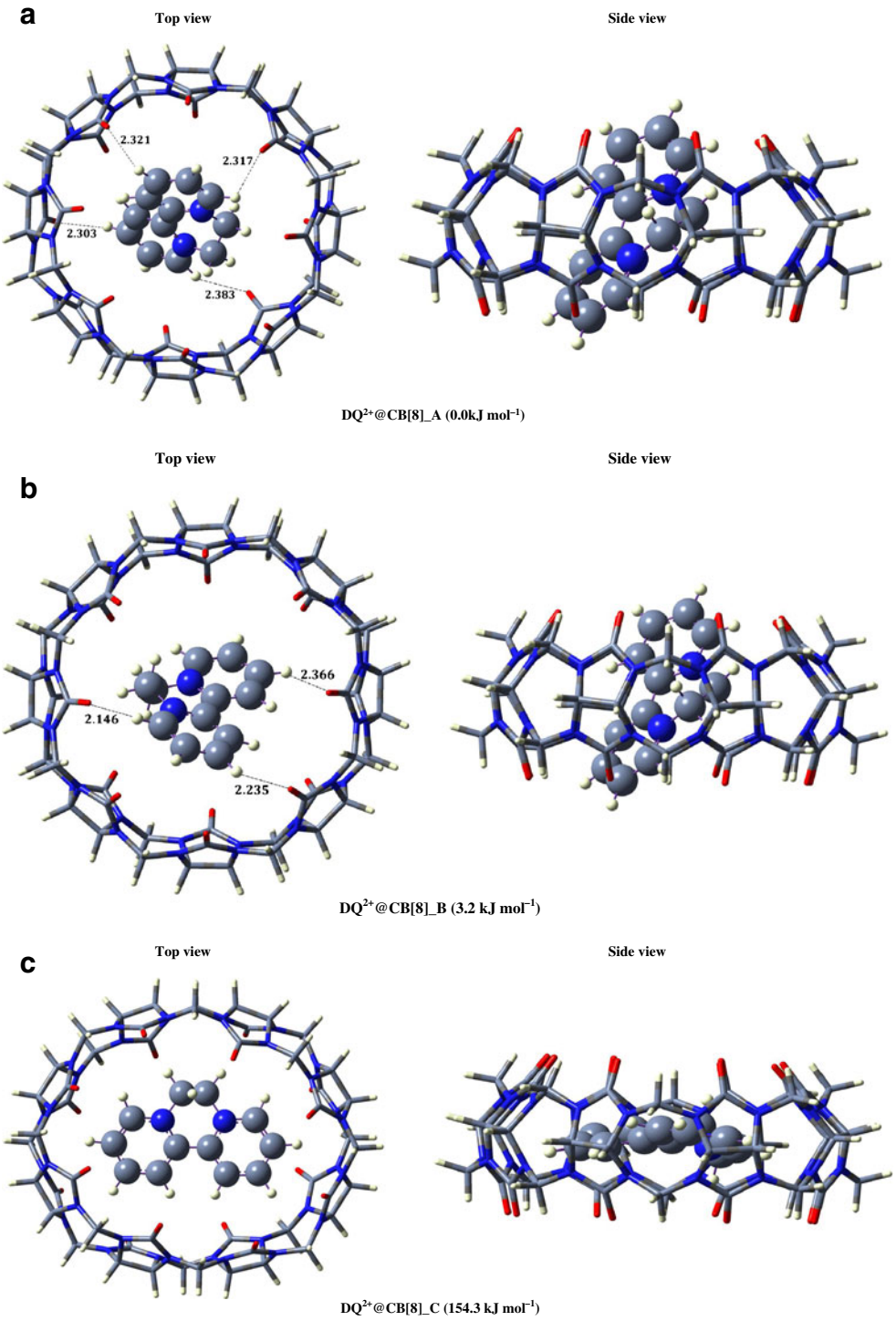

Fig. 3 B3LYP/6-31G(d,p) gas phase optimized geometries of 'A', 'B' and 'C' conformer of DQ^{2+}@CB[8] complex. The *blue* and *red* atoms denote nitrogen and oxygen centers

atoms around their equilibrium position. The harmonic vibrational frequencies are scaled [18] by a factor of 0.9614. The infrared spectra were obtained through a plot of the molar absorption coefficient (in the units of 0.1 m^2 mol^{-1}) that specifically designates a specific absorption versus the frequency (in cm^{-1}). For acuminous visualization, we employ the package GAUSSVIEW-5 [19]. The interaction energies were calculated by subtracting the sum of electronic energies of isolated hosts and DQ^{2+} guest from that of its complex. Natural bond orbital (NBO) analyses have further been carried out [20]. ^{1}H NMR

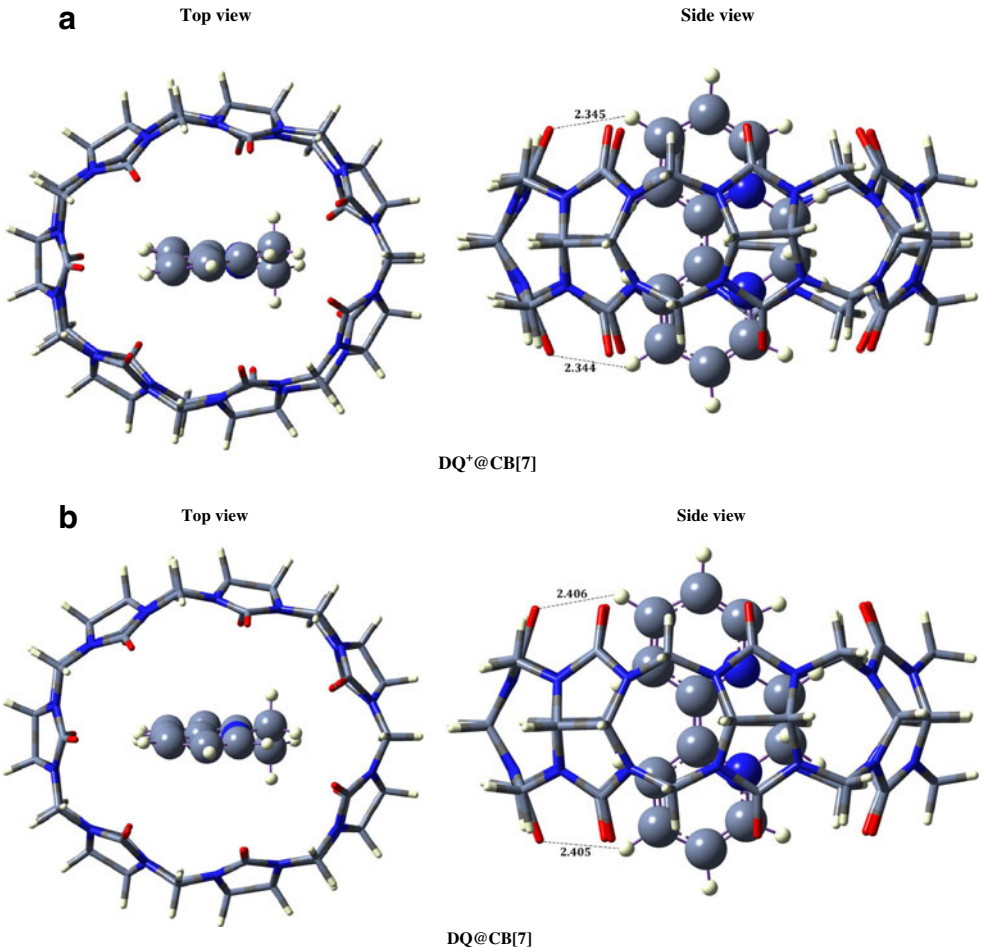

Fig. 4 B3LYP/6-31G(d,p) gas phase optimized geometries of **a** DQ^{+}@CB[7] **b** DQ@CB[7]

chemical shifts (δ_H) were calculated by subtracting the nuclear magnetic shielding tensors of protons in host, guests and their complex from those in the tetramethylsilane (reference) using the gauge-independent atomic orbital (GIAO) method [21] within the framework of density functional calculations incorporating all three exchange correlation functionals. Furthermore, the effect of solvent (water) on the electronic structure and ^{1}H NMR chemical shifts was modeled through self-consistent reaction field (SCRF) calculations with polarization continuum model (PCM) [22].

Results and discussion

Binding patterns and energetics

Cucurbituril monomer and DQ^{2+} (guest) are shown in Fig. 1 along with the atomic labeling scheme used. Exploring the molecular electrostatic potential (MESP) topography of CB[7] and CB[8] hosts different host–guest conformers were generated. MESP brings about electron-rich regions in the host and the critical points (minima) therein represent the potential binding sites for the guest [23]. Details of the MESP topography of isolated CB[n] hosts can be found in the literature [24]. The host–guest conformers were further subjected to optimizations within the frame work of B3LYP/6-31G(d,p) theory. It should be remarked here that the possible structures between DQ^{2+} and CB[7] exhibiting qualitatively different binding patterns finally converged to only one conformer in which DQ^{2+} encapsulates parallel to the cavity axis facilitating C=O···H interactions (2.270 and 2.271 Å) between the portal of the host and C–H_γ of the guest. Optimized structure of DQ^{2+}@CB[7] complex has been displayed in Fig. 2.

The relatively large cavity size of the host leads to three conformers ‘A’, ‘B’ and ‘C’ for the DQ^{2+}@CB[8] complex, which are shown in Fig. 3. In two of these conformers (‘A’ and ‘B’) DQ^{2+} orients parallel to the cavity axis facilitating hydrogen bonding interactions between α and γ-protons of DQ^{2+} guest with host portals. As may readily be noticed, the lowest

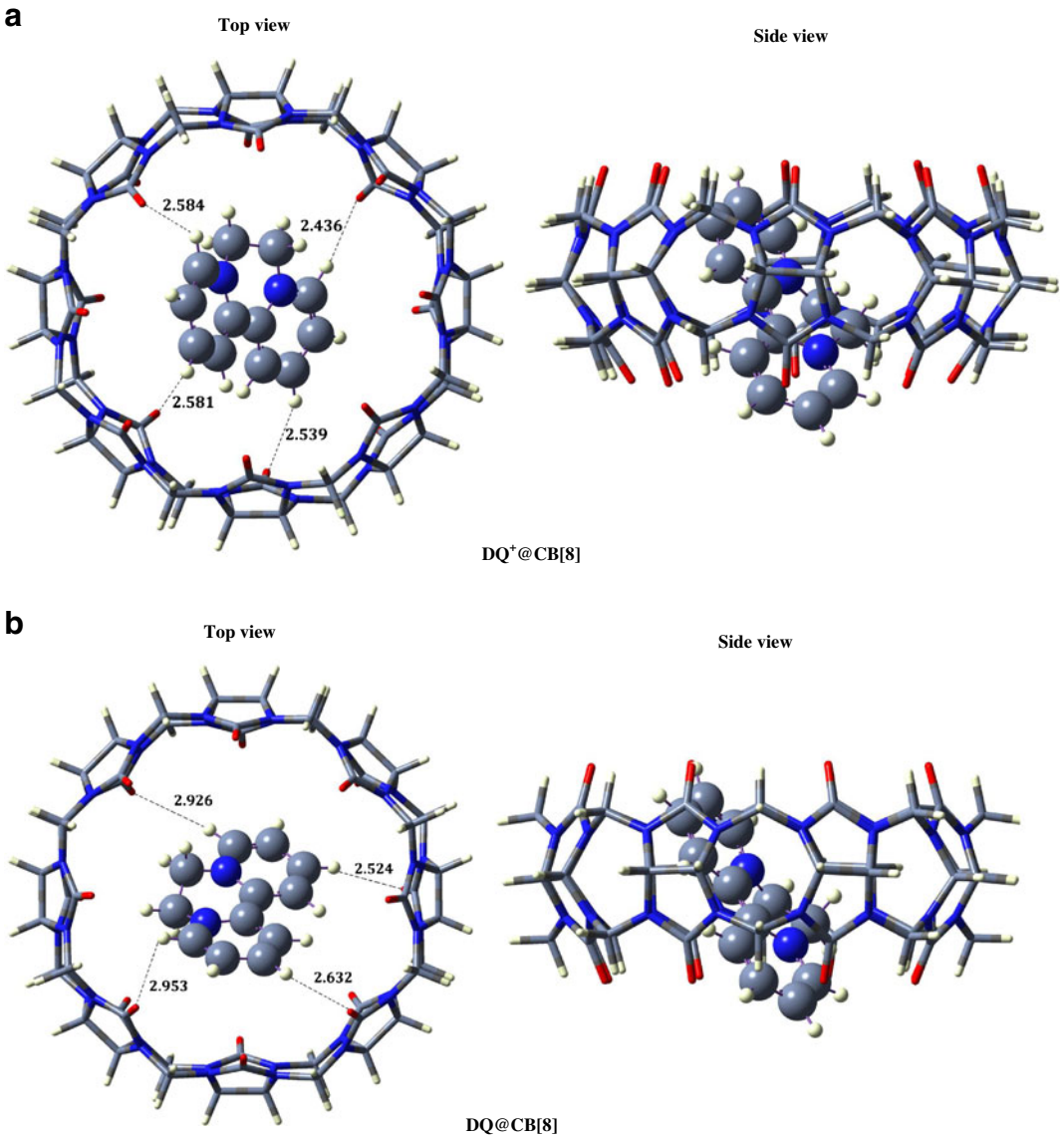

Fig. 5 B3LYP/6-31G(d,p) gas phase optimized geometries of **a** DQ^{+}@CB[8] **b** DQ@CB[8]

energy conformer 'A' possesses four such C=O···H interactions compared to three inferred for the conformer 'B'. The conformer 'C' reveals that the guest aligns perpendicular to the CB[8] axis brings about large cavity distortion and is void of hydrogen bonding interactions that results in destabilization of ~154 kJ mol^{-1} (over 'A') for this conformer. It may thus be conjectured that number of hydrogen bonded interaction results in lowering of energy of the complex.

Electronic structures of DQ^{2+}@-CB[7] and -CB[8] complexes following two step one electron reduction leading to reduced cation and neutral species were characterized (cf. Figs. 4 and 5). It has been observed that the host–guest binding is qualitatively the same in all these complexes. Aromatic rings of DQ^{2+} tend to attain planarity on transformation of di-cation to neutral species along the two-step reduction. Hydrogen bond distances in DQ^{2+}@CB[7] and DQ^{2+}@CB[8] with their respective reduced cation and neutral complexes are shown in Table 1S of the supporting information. The complexes of the reduced species possess relatively longer hydrogen bond distances than those in di-cationic complexes. From Fig. 1S of supporting information it is transparent that host–guest binding pattern in the lowest energy host–guest complexes from B3LYP, B97D as well as PBE0 based calculations is qualitatively similar. The C=O···H bond distances in the DQ^{2+}@CB[7] complex from the B3LYP calculations agree well with those incorporating PBE0 functional; the corresponding distances from the B97D based calculations are predicted to be 0.0127 Å longer. Likewise C=O···H bond distances in DQ^{2+}@CB[8]

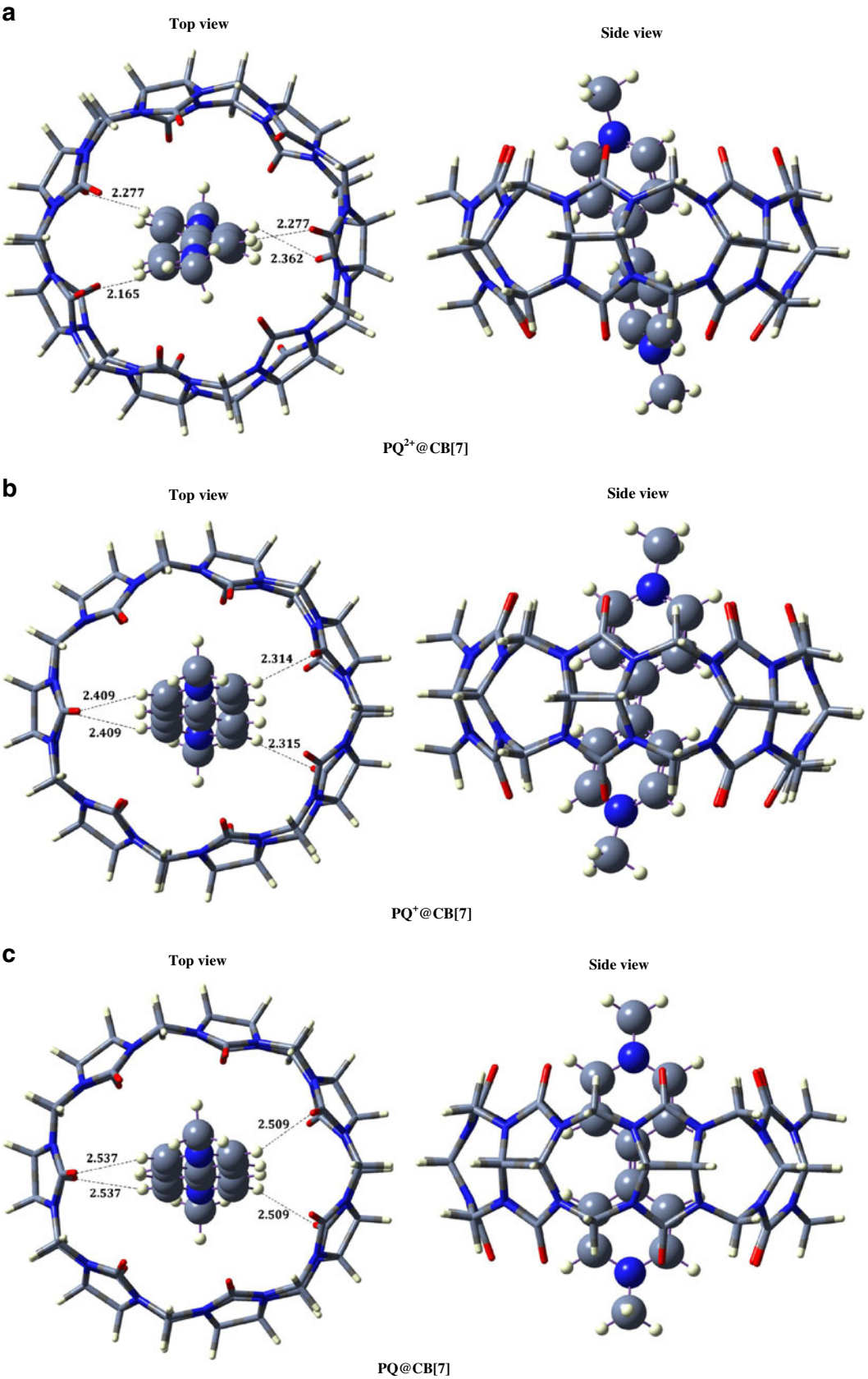

Fig. 6 B3LYP optimized geometries of **a** PQ^{2+}@CB[7] **b** PQ^{+}@CB[7] **c** PQ@CB[7] **d** PQ^{2+}@CB[8] **e** PQ^{+}@CB[8] **f** PQ@CB[8]

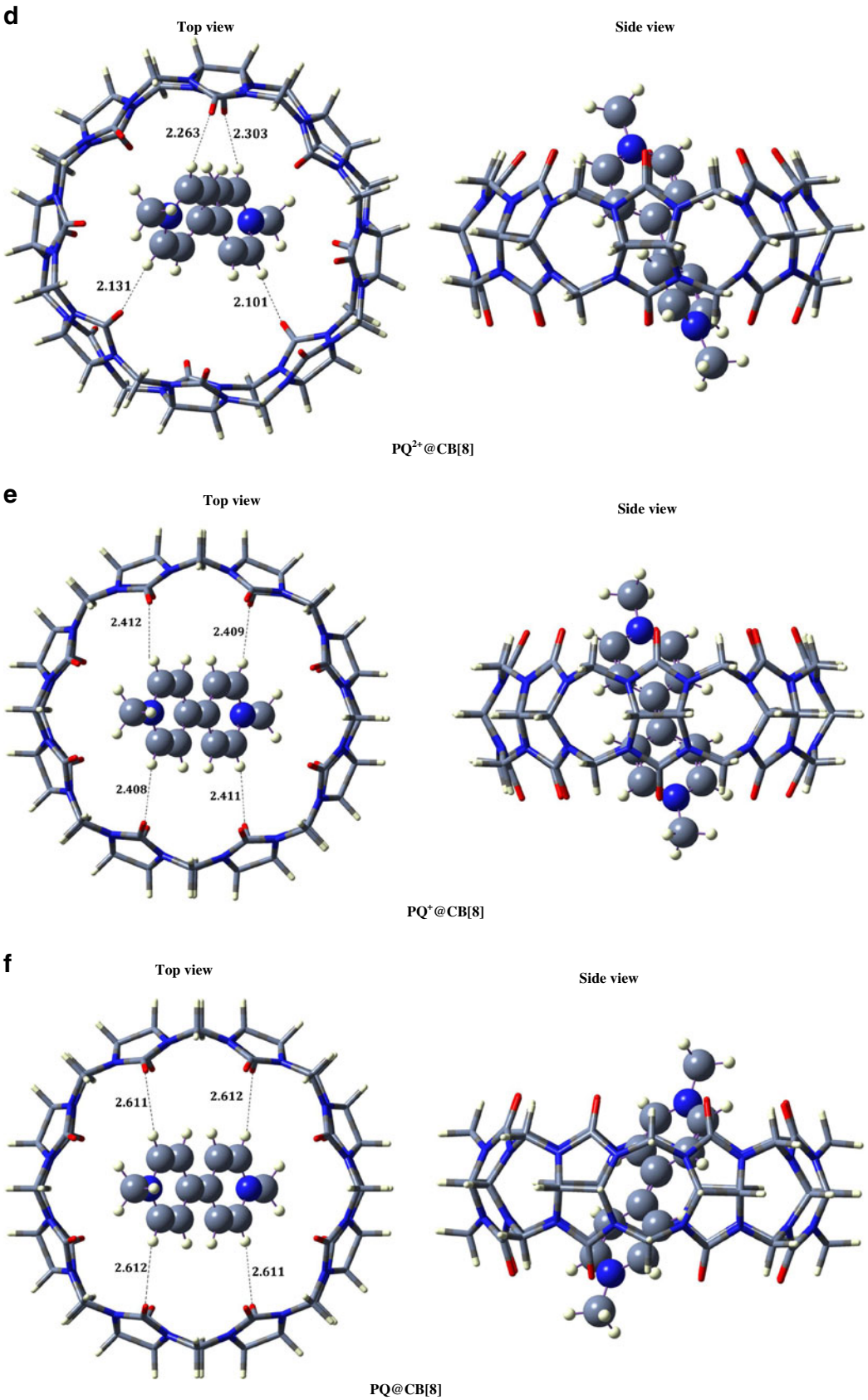

Fig. 6 (continued)

Table 1 Binding energy (ΔE_{bind} in kJ mol^{-1}), zero point corrected binding energy (ΔE_{zp} in kJ mol^{-1}), BSSE corrected binding energy (ΔE_{BSSE} in kJ mol^{-1}), change in Gibbs free energy (ΔG in kJ mol^{-1}), internal energy (ΔU in kcal mol^{-1}), enthalpy (ΔH in kJ mol^{-1}), entropy (ΔS cal/mol-Kelvin) of DQ^{n+} ($n = 2, 1, 0$) complexes with CB[7] and CB[8] host

	DQ@CB[7]							DQ@CB[8]						
	Di-cation			Cation		Neutral		Di-cation			Cation		Neutral	
	B3LYP	B97D	PBE0	B3LYP	B97D	B3LYP	B97D	PBE0	B3LYP	B97D	PBE0	B3LYP	B97D	PBE0	B3LYP	B97D	PBE0
ΔE_{bind}	450.0	630.0	478.7	183.9	351.5	207.5	3.0	160.2	21.6	454.3	606.4	480.5	200.0	335.7	210.3	23.4	154.1	37.4
ΔE_{zp}	104.7	612.0	468.5	42.3	338.4	202.1	0.03	151.7	19.8	106.1	587.6	470.1	46.2	322.7	205.4	4.9	144.5	35.9
ΔE_{BSSE}	78.7	538.7	399.2	35.4	255.6	127.5	9.8	51.3	65.9	85.6	508.9	409.6	48.9	236.9	146.3	27.4	49.0	39.2
ΔG	−88.0	−539.8	−403.0	−27.2	−183.6	−142.6	−13.2	−88.8	−32.9	−90.4	−498.3	−401.6	−32.4	−244.8	−200.7	−8.3	−68.3	−22.4
ΔH	104.6	613.8	467.7	41.9	338.7	200.1	0.6	151.2	16.9	105.9	590.2	470.0	45.7	323.2	195.6	4.2	144.3	33.4
ΔU	3.4	4.6	3.2	2.5	3.6	2.3	1.8	2.7	1.7	3.1	4.4	3.1	2.4	3.5	2.7	1.7	2.9	1.5
ΔS	−55.9	−59.3	−51.8	−49.1	−55.8	−46.1	−42.4	−49.9	−39.9	−52.1	−73.6	−54.8	−44.3	−62.8	−49.5	−42.1	−60.8	−44.7

complexes from the B97D based calculations are, respectively, 0.095 Å and 0.085 Å longer, compared to their B3LYP and PBE0 counterparts. Furthermore hydrogen bond distances in the mono-cation and neutral complexes lead to qualitatively similar inferences.

The influence of solvent (water) on host–guest binding patterns in DQ^{2+}@CB[7] and -CB[8] along with their reduced cation complexes was simulated through SCRF-PCM calculations. The qualitative trend of energies and hydrogen bond distances observed for the gas phase structures was conserved. The presence of solvent engenders relatively short C=O···H distances (by ~0.01 Å) in the complex compared to those in gas phase structures. Lowest energy complexes of DQ^{2+}@CB[7], -CB[8] and their reduced cation species are shown in Fig. 2S and Fig. 3S of the supporting information.

Viologen reveal two forms viz., paraquat (PQ^{2+}) and diquat. Experimental investigations in the literature [5, 9, 25–27] are largely focused on paraquat combined with CB[n] hosts. In this work we envisage binding of diquat to such hosts using density functional calculations based on different functionals and compare the binding of these two forms in terms of complexation energies. B3LYP optimized structures of PQ^{2+}@CB[7] or -CB[8] complexes are depicted in Fig. 6. The structure reveals that PQ^{2+} encapsulates within the CB[n] cavity facilitate hydrogen bonding interactions of methylene groups as well as α-hydrogens with ureido oxygens of the host portals.

Calculated interaction energies as well as thermodynamic parameters accompanying complexation are given in Table 1. Stronger binding of DQ^{2+} is evident from the change in Gibbs free energy (ΔG) parameters reported therein. Interestingly ΔG values of the DQ^{2+} @CB[8] complex employing B3LYP, B97D and PBE0 functionals follow the order: B97D(−498.3) < PBE0 (−401.6) < B3LYP (−90.4); which is parallel to binding energies displayed in this table. Nonetheless, the calculations incorporating B97D functional predicted binding energy for DQ^{2+}@CB[7] complex to be ~220 kJ mol^{-1} larger than that from B3LYP theory. As shown here, binding energy from PBE0 based calculations turns out to be 478 kJ mol^{-1} which compares well with its B3LYP counterpart (450 kJ mol^{-1}). Similar conclusions were drawn in case of the DQ^{2+}@CB[7] complex from the data reported in Table 1. BSSE corrected energies are also reported in Table 1.

Kaifer et al. [8] elucidated X-ray crystal structures of DQ^{2+} complexes with CB[8]. The structures of the DQ^{2+} complex from B3LYP, B97D or PBE0 calculations by and large, agree well with the X-ray crystal structure data.

Binding energies data on 1:1 complex of PQ^{2+} and CB[7] or CB[8] host are given in Table 2S of the supporting information, points to stronger affinity of PQ^{2+} toward CB[n] hosts. This partly can be attributed to the separation of electron-deficient nitrogen's in PQ^{2+} (7.055 Å) in

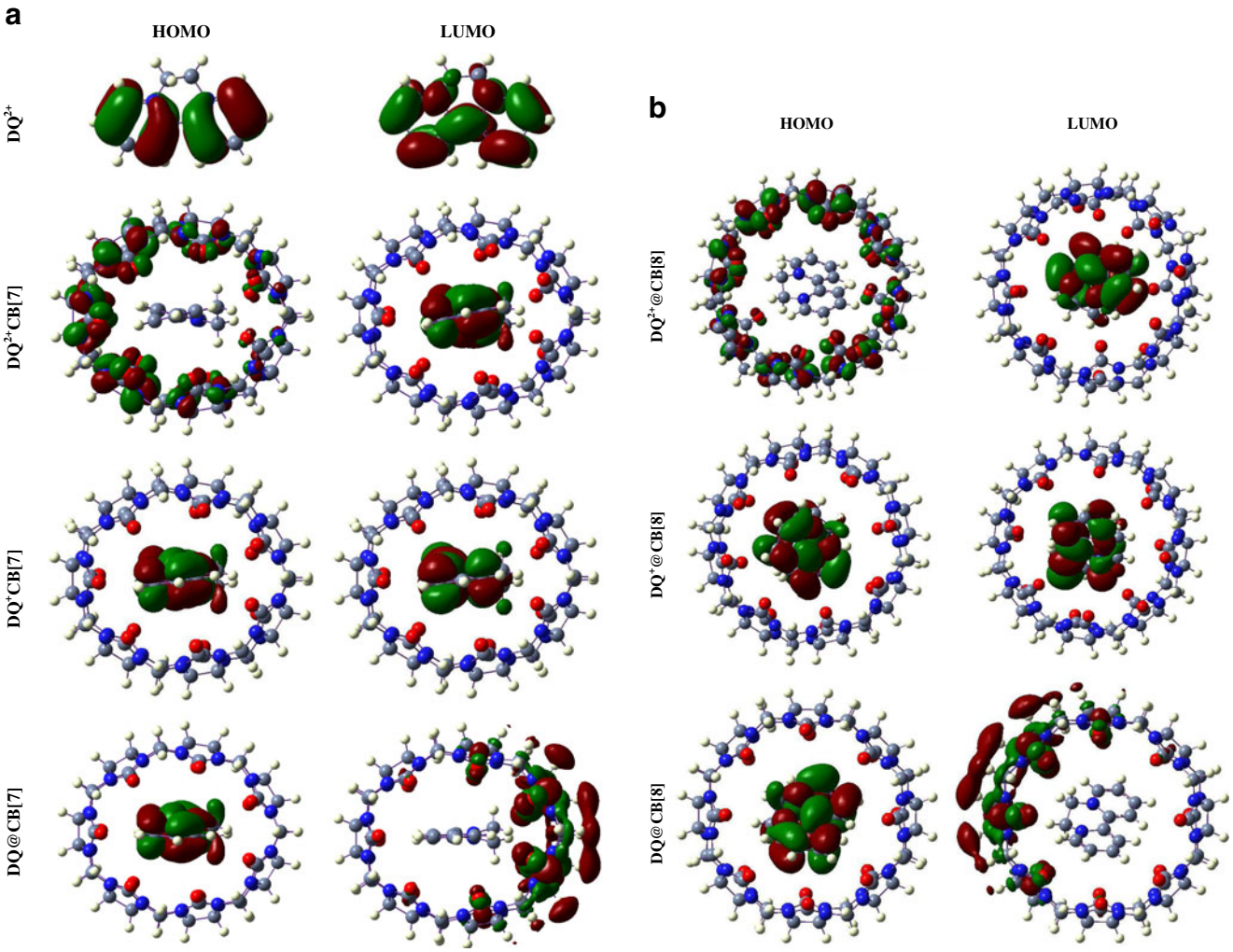

Fig. 7 Frontier orbitals (HOMO and LUMO) in DQ^{2+}@CB[7] and CB[8] host and their two step one electron reduction complexes

the complexes which match well with the cavity-heights of CB[7] or CB[8] cavitands estimated from the calculations [24].

To understand how solvent influences electronic structure, SCRF-PCM optimizations were carried out. Selected geometrical parameters in CB[n] hosts and their DQ^{2+} as well as reduced cation complexes are compared from density functional calculations incorporating B3LYP, B97D and PBE0 functionals in Table 3S of the supporting information. Thus, the B3LYP calculated values fall in between those of B97D and PBE0 functionals. Accordingly carbonyl bond distances in the isolated CB[8] host using different functionals follows the order: B97D (1.219 Å) > B3LYP (1.213 Å) > PBE0 (1.209 Å).

The complexation of CB[n] with DQ^{n+} influences C=O bond distances in the isolated host. As may further be noticed C=O bonds are elongated in the DQ^{2+}@CB[8] complex (1.218 Å). On the other hand, shortening of C–N bond can be noticed for DQ^{2+} as well as in its reduced cation (or neutral) complexes. Encapsulation of di-cation thus engenders contraction of host-cavity bringing radial opposite oxygens (O1–O1*) closer (9.830 Å) than those in the isolated CB[8] (10.299 Å) (O1 and O1* refer to radial opposite oxygen atoms from neighboring glycouril monomers in the CB[n] host). The cavity size was found to be nearly unchanged in the reduced cation complexes (cf. Fig. 5).

Frontier orbitals

Frontier orbitals (HOMO and LUMO) in isolated CB[7], CB[8] hosts, DQ^{2+} guest and their complexes are depicted in Fig. 7. The HOMO in the DQ^{2+}@CB[8] complex has largely been localized near the host. On the contrary, the DQ@CB[8] complex reveals that its HOMO resides solely on the neutral guest. The charge transfer subsequent to reduction is thus evident. HOMO-LUMO energy separation in host–guest complex on reduction decreases steadily from 3.0 eV in the DQ^{2+} complex to 2.2 eV.

Table 2 ^{1}HNMR chemical shifts in isolated CB[7] and CB[8] hosts and their DQ^{n+} (n=2, 1, 0) complexes

	B3LYP		B97D		PBE0		B3LYP						B97D						PBE0					
							Di-cation		Cation		Neutral		Di-cation		Cation		Neutral		Di-cation		Cation		Neutral	
	Gas	Water	Gas	Water	Gas	Water	Gas	Water	Gas	Water	Gas	Water	Gas	Water	Gas	Water	Gas	Water	Gas	Water	Gas	Water	Gas	Water
	CB[7]						DQ@CB[7]																	
H_1	3.0	3.8	3.2	3.7	3.2	3.7	3.3	3.8	3.2	3.8	3.3	3.8	3.4	3.8	3.3	3.7	3.2	3.3	3.5	3.8	3.4	3.8	3.5	3.8
H_2	4.4	5.3	4.5	4.9	4.5	5.0	4.5	5.0	4.5	5.0	4.4	5.0	4.6	5.0	4.5	4.9	4.5	4.3	4.7	5.0	4.6	5.0	4.5	5.0
H_3	6.0	5.8	6.2	5.6	6.5	5.8	5.8	5.7	5.7	5.7	5.7	5.8	5.9	5.7	6.0	5.6	6.2	5.0	6.1	5.8	6.0	5.8	5.9	5.9
	CB[8]						DQ@CB[8]																	
H_1	3.0	3.8	3.2	3.7	3.2	3.7	3.2	3.8	3.2	3.8	3.0	3.8	3.5	3.7	3.4	3.8	3.2	3.3	3.5	3.8	3.4	3.6	3.2	3.7
H_2	4.2	5.2	4.4	4.9	4.4	4.9	4.5	4.9	4.4	5.0	4.3	5.0	4.6	5.0	4.5	4.9	4.4	4.9	4.6	5.0	4.6	4.9	4.5	5.0
H_3	6.0	5.8	6.2	5.6	6.5	5.9	5.8	5.8	5.9	5.8	6.0	5.8	6.0	5.8	6.1	5.7	6.2	5.7	6.3	5.9	6.4	5.8	6.5	5.9

B3LYP—gas-31.7598, water-31.7352

B97D—gas-31.5743, water-31.5589

PBE0—gas-31.6653, water-31.6433

Table 3 ^{1}HNMR chemical shifts in water for isolated DQ^{2+} and their complexes with CB[7] and CB[8] hosts

	B3LYP		B97D		PBE0		B3LYP						B97D						PBE0					
							Di-cation		Cation		Neutral		Di-cation		Cation		Neutral		Di-cation		Cation		Neutral	
	Gas	Water	Gas	Water	Gas	Water	Gas	Water	Gas	Water	Gas	Water	Gas	Water	Gas	Water	Gas	Water	Gas	Water	Gas	Water	Gas	Water
	DQ^{2+}						DQ@CB[7]																	
H_α	8.9	9.3	8.5	8.5	8.9	8.9	9.2	9.2	7.2	7.1	5.5	5.7	8.9	8.7	7.0	7.1	5.3	5.6	9.2	9.1	7.3	7.3	5.6	5.9
H_β	9.0	8.7	8.7	8.2	9.0	8.6	8.5	8.3	6.4	6.2	4.6	4.2	8.2	8.1	6.1	6.0	4.3	4.1	8.6	8.5	6.5	6.3	4.5	4.4
H_γ	9.5	9.1	9.1	8.7	9.6	9.1	9.8	9.7[a]	7.6	7.3	5.7	5.4	9.5	9.1	7.1	6.9	5.2	5.1	9.9	9.7	7.7	7.5	5.8	5.6
H_δ	9.1	9.2	8.6	8.6	9.0	9.0	8.0	8.1	6.1	6.5	4.6	5.0	7.6	7.8	6.0	6.4	4.7	4.9	7.9	8.2	6.3	6.7	4.9	5.1
H_a	4.8	5.1	4.9	4.9	5.0	5.0	4.5	4.6	3.2	3.5	2.3	2.4	4.5	4.7	3.4	3.6	2.4	2.6	4.5	4.6	3.3	3.5	2.3	2.4
	DQ^{2+}						DQ@CB[8]																	
H_α	8.9	9.3	8.5	8.5	8.9	8.9	9.5	9.7[a]	7.2	7.5	5.3	5.6	8.9	8.8	7.0	7.0	5.0	5.5	9.7	9.6	7.3	7.2	5.4	5.6
H_β	9.0	8.7	8.7	8.2	9.0	8.6	9.0	8.4	6.6	6.3	4.4	4.3	8.2	8.0	6.8	6.7	4.7	4.7	9.0	8.6	6.8	6.5	4.5	4.4
H_γ	9.5	9.1	9.1	8.7	9.6	9.1	9.7	9.2	7.3	7.0	5.3	5.2	9.4	9.2	7.0	6.9	5.0	5.1	9.9	9.4	7.4	7.2	5.4	5.3
H_δ	9.1	9.2	8.6	8.6	9.0	9.0	8.4	8.2	6.8	6.7	5.2	5.2	7.6	7.9	6.6	6.6	5.2	5.3	8.5	8.4	6.9	7.1	5.3	5.4
H_a	4.8	5.1	4.9	4.9	5.0	5.0	4.4	4.5	3.3	3.5	2.2	2.4	4.6	4.7	3.5	3.6	2.5	2.5	4.6	4.6	3.5	3.6	2.4	2.5

B3LYP—gas-31.7598, water-31.7352, B97D—gas-31.5743, water-31.5589, PBE0—gas-31.6653, water-31.643

[a] Proton participating in hydrogen bonding

Table 4 Selected vibrational frequencies (ν = stretching and δ = bending) of CB[7] and CB[8] host and their complexes with DQ^{2+}. Intensities (in km. mol^{-1}) are given in parentheses

Assignment	CB[7]	CB[8]	DQ^{2+}@CB[7]	DQ^{2+}@CB[8]
ν (CH_2)	2892(188)	3011(52)	2885(43)	2877(36)
			2938(107)	2909(33)
ν (CH)	2885(214)	2879(729)	2924(114)	2930(110)
				2919(69)
ν (C=O)	1791(3585)	1788(4251)	1772(1831)	1765(1465)
			1776(855)	1792(1250)
CH_2 wag	1422(1413)	1422(1559)	1422(952)	1427(803)
	1374(53)	1370(118)	1425(910)	1376(97)
		1351(602)	1380(43)	
CH_2 scissor + CH twist	1420(69)	1423(46)	1419(156)	1438(78)
			1423(80)	1421(330)
CH_2 scissor	1402(23)	1415(214)	1399(44)	1417(234)
	1406(75)	1410(153)	1404(132)	1419(213)
	1410(59)		1412(111)	1406(156)
CH wag	1363(171)	1365(268)	1369(40)	1355(154)
		1222(483)	1353(112)	1222(166)
			1358(37)	
ν (N3–C4–N5)	1272(668)	1271(794)	1262(400)	1263(202)
	1259(181)	1258(193)	1257(57)	1255(109)
CH rock	1163(765)	1190(1929)	1158(655)	1190(1207)
	1190(1405)	1165(975)	1187(78)	1188(1161)
			1193(1065)	1157(898)
CH_2 rock	953(517)	958(659)	938(112)	946(124)
			940(202)	962(56)
H–C–C–H deformation	776(955)	780(1225)	773(367)	778(744)
			778(566)	797(303)
N–C–O deformation	716(116)	715(114)	749(112)	715(12)
				715(21)
				719(86)
N–C–N breathing	416(23)	414(26)	436(10)	416(12)
CH_2 rock	347 (110)	345(88)	360(63)	357(92)
	346(80)	347(80)	363(28)	361(78)
N–C–O deformation	93(8)	95(17)	99(13)	110(30)

^{1}H NMR spectra

^{1}H NMR chemical shift (δ_H) of DQ^{2+} guest follow the order: H_γ (9.5 ppm) > H_δ (9.1 ppm) > H_β (9.0 ppm) > H_α (8.9 ppm). Experimental NMR spectra reveal that H_α protons are more de-shielded than H_δ or H_γ protons. In other words, gas phase calculated δ_H values do not qualitatively agree with the experiment. It should be remarked here that Bagno [28] has pointed out that the solvent influences the chemical shift significantly. It was further concluded that δ_H values from SCRF calculations agree better with those from the measured NMR spectra than for the gas phase calculations or those simulated by incorporating explicit solvent molecules. Pursuant to this, the chemical shifts in DQ^{2+}, CB[n] hosts and their complexes were calculated in the presence of water (solvent). SCRF simulated NMR data on the DQ^{2+}@-CB[7] or CB[8] complexes from the B3LYP theory lead to δ_H values consistent with the experimental NMR [8]. A comparison of δ_H values in the calculated ^{1}H NMR spectra using B97D functional within the realm of SCRF-PCM theory, however, reveal the order: $H_\gamma > H_\delta > H_\beta > H_\alpha$ which is qualitatively different from that observed in experiment [8]. Moreover, the chemical shifts in ^{1}H NMR from PBE0 calculations do not agree qualitatively with the experimental data. The better agreement of B3LYP derived NMR chemical shifts data with those from experiment was also noticed earlier in complexation of babmus[6]uril host [29]. In other words it may be conjectured that how the host–guest complexation reflect in chemical shifts in ^{1}H NMR spectra is well described through the use of the B3LYP functional. In the

Table 5 Selected vibrational frequencies (ν = stretching and δ = bending) of DQ^{2+} and their complexes with CB[7] and CB[8] hosts. Intensities (in km. mol^{-1}) are given in parentheses. [a]Asymmetric stretching vibrations

Assignment	DQ^{2+}	DQ^{2+}@CB[7]	DQ^{2+}@CB[8]
ν (CH)	3119(53)	3128(25)	3078(115)α
		3116(80)	3100(90)α
			3132(19)β
$\nu (CH)_\delta$	3126(14)	3133(7)	3144(10)δ
$\nu (CH_2)$	2966(1)	2964(1)	2959(5)
	3046(3)[a]	3069(18)[a]	3028(27)[a]
ν (C=C)	1579(94)	1583(143)	1578(156)
δ (CH) + CH_2 scissor	1475(117)	1483(77)	1481(90)
CH_2 scissor	1429(16)	1431(28)	1446(40)
			1433(221)
CH_2 wagg	1342(12)	1348(69)	1355(154)
	1285(41)	1292(14)	1377(39)
			1289(56)
CH rock	1301(27)	1317(5)	1314(37)
			1414(15)
CH_2 twist	1216(20)	1208(7)	1216(9)
			1231(18)
C–H scissor	1161(7)	1166(46)	1160(34)
ν (C–N)	1160(40)	1170(65)	1166(21)
δ(CH)	1126(11)	1131(13)	1132(8)
C_1–C_3–C_5 breath	1008(9)	1047(1)	1007(8)
C–H wagg	765(89)	760(17)	758(21)
	695(18)	753(37)	754(49)
		689(24)	689(15)
C_5–$C_{5'}$ deformation + C–H wagg	457(11)	464(13)	459(17)
	190(7)	195(8)	196(4)

following we restrict our discussion to the results derived from the B3LYP theory.

CB[7]/CB[8] monomer possesses three different types of protons H_1, H_2 and H_3 (depicted in Fig. 1). In Table 2, we compare the δ_H values of host protons with those in the DQ^{2+} complex. As may be noticed, δ_H values of α-protons of the DQ^{2+} from the SCRF-PCM theory generally reveal downfield signals. The δ_H signals due to aliphatic substituent (N–CH_2) are observed near 5.1 ppm. The inferences borne out from the B3LYP calculations are in consonant with the experiment.

The ^1H NMR chemical shifts of isolated guest and their lowest energy complexes are reported in Table 3. As shown, both H_δ (protons encapsulated inside the cavity) and H_β (residing near the CB[8] portal) reveal significant shielding and alters the corresponding ($\Delta\delta_H$) signals by ~1.0 ppm and 0.5 ppm. As opposed to this, H_α protons interacting with ureido oxygens of the host exhibit deshielding ($\Delta\delta_H$~ 0.4 ppm) in the calculated NMR. Contrary to the B3LYP calculations, the order of the δ_H signals in the ^1H NMR of DQ^{2+}@CB[8] complex borne out from the B97D/6-31+G(d,p) computations in the presence of solvent (water) do not qualitatively agree with those from the experiment. This is evident from the data reported in Table 4S of the supporting information.

Vibrational frequencies

Calculated vibrational frequencies in DQ^{2+}@CB[7] and CB[8] complexes are compared with those in the corresponding isolated host and the guest in Tables 4 and 5. The vibrational spectra of CB[7] or CB[8] complex in (a) 2800–3300 cm^{-1} (b) 1000–2000 cm^{-1} (c) 500–900 cm^{-1} and lastly (d) below 500 cm^{-1} regions, are shown in Figs. 8

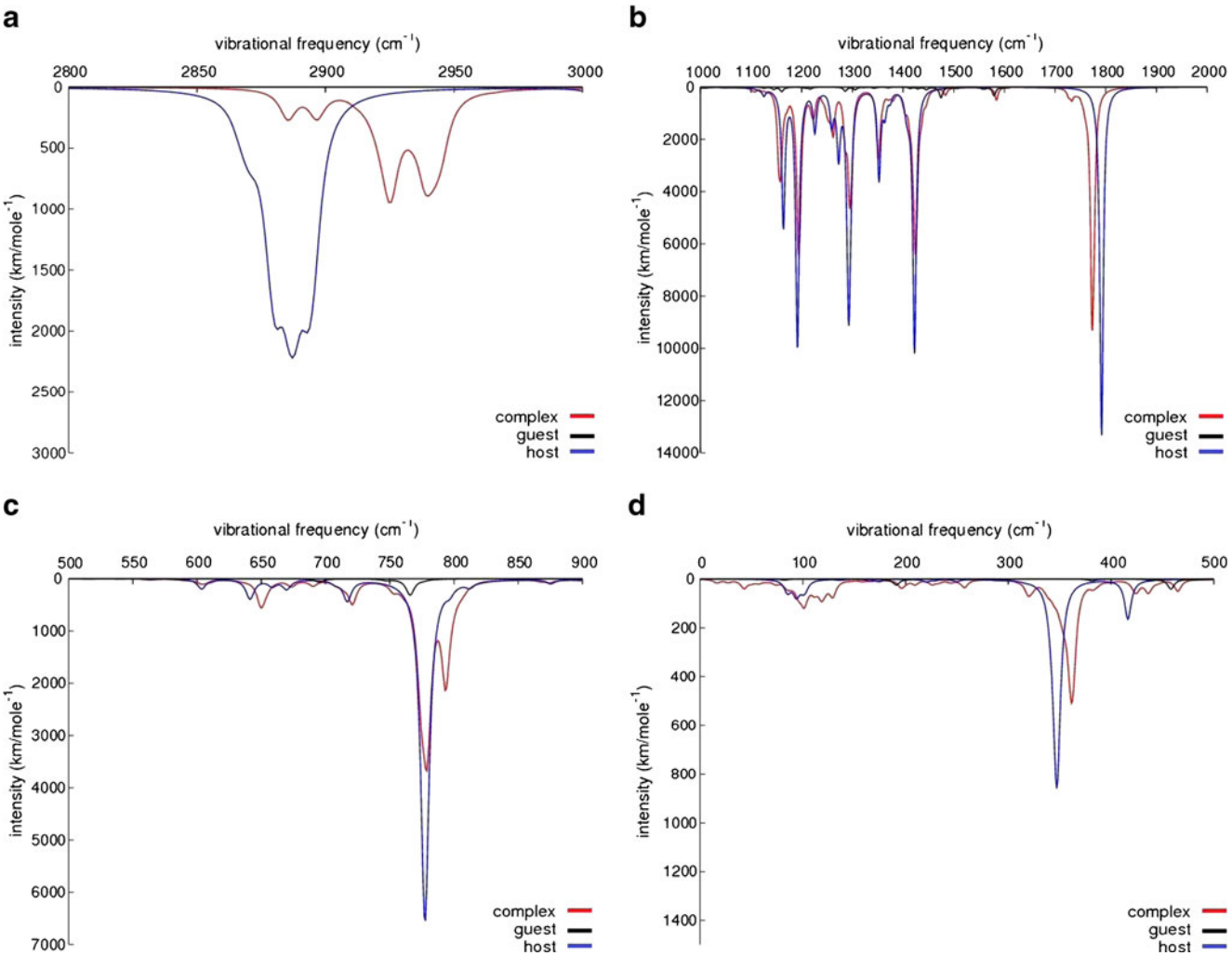

Fig. 8 Vibrational spectra of DQ^{2+}@CB[7] complexes in **a** 3300–2800 cm^{-1} **b** 1700–500 cm^{-1} **c** 900–500 cm^{-1} and **d** below 500 cm^{-1} regions

and 9. The normal vibrations of DQ^{2+}@CB[8] from the B3LYP theory, are discussed as a proto type example, in the following.

As shown in Fig. 9a, aromatic C–H vibrations of isolated DQ^{2+} correspond to 3119 cm^{-1} (H_β) and 3126 cm^{-1} (H_δ) on complexation exhibit frequency blue-shift. The corresponding vibrations of the complex are assigned to 3132 cm^{-1} and 3144 cm^{-1}, respectively. The methine (CH) stretching of the CB[8] viz., 2879 cm^{-1} vibration exhibits a blue shift of 51 cm^{-1} on complexation. On the other hand, H_α protons from hydrogen bonding engender an intense band on complexation and the corresponding frequency red-shift falls in between 19 cm^{-1} to 41 cm^{-1}. Likewise, the methylene (CH_2) vibration of DQ^{2+} shifts to lower wavenumber (2966 cm^{-1}) in the DQ^{2+}@CB[8] complex. The intense C=O stretching vibration of the isolated CB[8] host is predicted near 1788 cm^{-1}. Complexation of CB[8] is further accompanied with splitting of distinct band for hydrogen bonded carbonyls (1765 cm^{-1}) and that for non-interacting one (1792 cm^{-1}). It may as well be remarked here that such splitting of C=O stretching was also observed on complexation of CB[8] with PQ^{2+}; the 1755 cm^{-1} vibration results from hydrogen bonding interactions. Moreover, splitting of 37 cm^{-1} in carbonyl stretching imply C=O···H interactions in the PQ^{2+} complex. Stronger binding with the host was, therefore, inferred [30].

As pointed out in the preceding section, NBO approach has been used to analyze the variation in the strength of different bonds accompanying the complexation of DQ^{2+} with CB[8]. The electron density in the anti-bonding natural orbital (σ^*), corresponding vibrational frequency and bond distances data are summarized in Table 6. As may readily be noticed, enhanced electron density in anti-bonding natural orbital engenders bond weakening and hence, the shift of frequency to lower wave number (red-shift). Thus, interactions between C=O and α-hydrogen of DQ^{2+} reveal increased electron

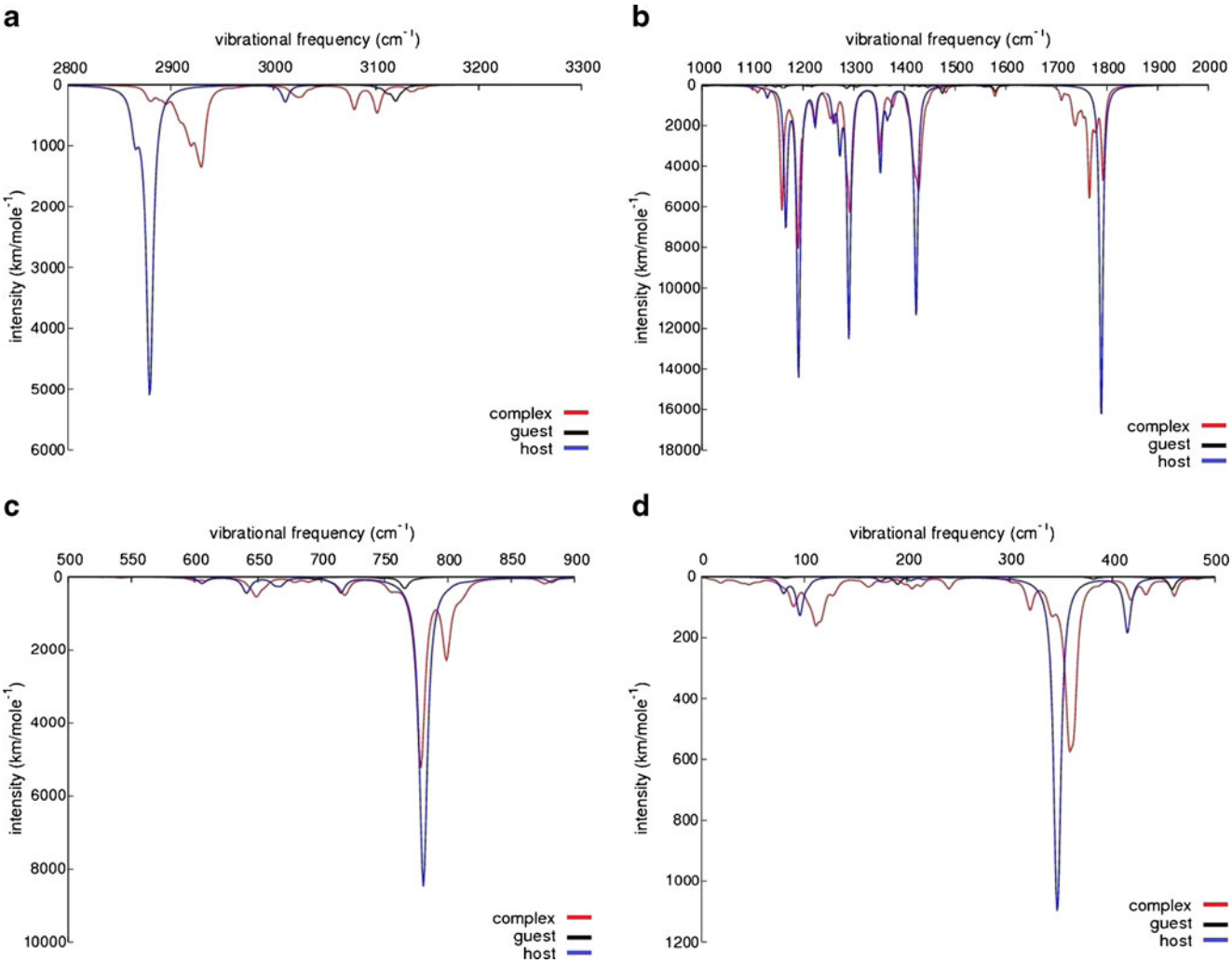

Fig. 9 Vibrational spectra of DQ^{2+}@CB[8] complexes in **a** 3300–2800 cm^{-1} **b** 1700–500 cm^{-1} **c** 900–500 cm^{-1} and **d** below 500 cm^{-1} regions

density from 0.1939 au to 0.1978 au, for the corresponding σ^* orbital. On parallel lines, the C–N vibration frequency of DQ^{2+} can be rationalized from the diminutive population (from 0.0391 au of isolated DQ^{2+} to 0.0288 au in the complex) of the corresponding C–N σ^* orbital.

The infra red spectra of CB[8] host in the region 1500 cm^{-1} to 1350 cm^{-1} (cf. Fig. 9b) shows intense bands at 1422 cm^{-1} and 1370 cm^{-1} which are blue-shifted by 5–6 cm^{-1}. These strong bands invoke strong coupling from different internal coordinates. The 1352 cm^{-1} band disappears on complexation. The ~780 cm^{-1} vibration of the isolated CB[8] and in the complex results from glycouril monomer of the CB[8] (cf. Fig. 9c). The additional 797 cm^{-1} band shows up in the infrared spectra of DQ^{2+}@CB[8] complex. Below 500 cm^{-1} region, the calculated infrared spectra of the isolated CB[8] show intense bands near 345 cm^{-1} and 347 cm^{-1}, those arise

Table 6 Electron density in anti-bonding orbital (σ* in au), bond distances (r in Å), and frequency of vibration (ν in cm^{-1}) in cucurbituril hosts, unbound DQ^{2+} guest and their complexes

					DQ^{2+}@CB[7]			DQ^{2+}@CB[8]		
		σ*	r	ν	σ*	r	ν	σ*	r	ν
CB[7]	C=O	0.1820	1.213	1791	0.1906	1.218	1740			
CB[8]	C=O	0.1939	1.213	1788	0.1978	1.218	1765			
DQ^{2+}	C–Hα	0.0100	1.084	3118	0.0165	1.084	3116			
	C–Hγ	0.0100	1.085	3118				0.0178	1.086	3102
	C–N	0.0391	1.488	1160	0.0292	1.479	1170	0.0288	1.483	1166

from the CH_2 vibrations. On complexation with DQ^{2+}, these vibrations emerge as a doublet with a separation of 4 cm^{-1} (near 360 cm^{-1}) in the spectra (cf. Fig. 9d).

Selected vibration frequencies in the DQ^{2+}@CB[8] complexes along with those of reduced cation DQ^{+} or neutral DQ are given in Table 5S of the supporting information. The blue shift of the C–N stretching vibration is evident for the complexes encapsulating the reduced cation.

Conclusions

Systematic investigations of DQ^{2+} guest with CB[n] (n = 7 and 8) hosts are carried out using density functional theory incorporating B3LYP, PBE0 and B97D functionals. It has been shown that the guest penetrates completely inside the host cavity facilitating interactions between H_α/H_γ of the DQ^{2+} and portal ureido oxygens of the host. CB[8] host binds more strongly to DQ^{2+}. B3LYP calculated ^{1}H NMR chemical shifts for DQ^{2+}@CB[8] complex in the presence of solvent (water) points to deshielding of H_α protons owing to hydrogen bonding interactions. Calculated infrared spectra reveal that the CN stretching exhibits a blue-shift of 6 cm^{-1} on encapsulation of DQ^{2+} within the CB[8] cavity. Likewise, aromatic C–H stretching arising from the guest protons residing within the host cavity engenders frequency blue-shift in the spectra of the DQ^{2+}@CB[8] complex. These inferences are supported by NBO analyses.

Acknowledgments SPG is grateful to the University Grants Commission (UGC), New Delhi, India [Research Project F34-370/2008(SR)].

References

1. Summers LA (1980) The bipyridinium herbicides. Academic, New York
2. Bird CL, Kubn AT (1981) Chem Soc Rev 10:49
3. Porter WW, Vaid TP (2005) J Org Chem 70:5028
4. Monk PMS (1988) The viologen synthesis, physicochemical properties and applications of the salts of 4,4′-dipyridinie. Wiley, Chichester
5. Ong W, Gomez-Kaifer M, Kaifer AE (2002) Org Lett 4:1791
6. Bersier PM, Bersier J, Klingert B (1991) Electroanalysis 3:443
7. Guo D-S, Wang L-H, Liu Y (2007) J Org Chem 72:7775
8. Ling Y, Mague JT, Kaifer AE (2007) Chem Eur J 13:7908
9. Jeon YJ, Kim HJ, Lee C, Kim K (2002) Chem Commun 1828
10. El-Barghouthi MI, Assaf KI, Rawashdeh AMM (2010) J Chem Theory Comput 6:984
11. Frisch MJ, Trucks GW, Schlegel HB, Scuseria GE, Robb MA, Cheeseman JR, Scalmani G, Barone V, Mennucci B, Petersson GA, Nakatsuji H, Caricato M, Li X, Hratchian HP, Izmaylov AF, Bloino J, Zheng G, Sonnenberg JL, Hada M, Ehara M, Toyota K, Fukuda R, Hasegawa J, Ishida M, Nakajima T, Honda Y, Kitao O, Nakai H, Vreven T, Montgomery JA Jr, Peralta JE, Ogliaro F, Bearpark M, Heyd JJ, Brothers E, Kudin KN, Staroverov VN, Kobayashi R, Normand J, Raghavachari K, Rendell A, Burant JC, Iyengar SS, Tomasi J, Cossi M, Rega N, Millam JM, Klene M, Knox JE, Cross JB, Bakken V, Adamo C, Jaramillo J, Gomperts R, Stratmann RE, Yazyev O, Austin AJ, Cammi R, Pomelli C, Ochterski JW, Martin RL, Morokuma K, Zakrzewski VG, Voth GA, Salvador P, Dannenberg JJ, Dapprich S, Daniels AD, Farkas O, Foresman JB, Ortiz JV, Cioslowski J, Fox DJ (2009) Gaussian 09, ReVision A.02. Gaussian, Inc., Wallingford
12. Becke AD (1988) Phys Rev A 38:3098
13. Lee C, Yang W, Parr RG (1988) Phys Rev B 37:785
14. Grimme SJ (2006) Comput Chem 27:1787
15. Perdew JP, Burke K, Ernzerhof M (1996) Phys Rev Lett 77: 3865
16. Perdew JP, Burke K, Ernzerhof M (1997) Phys Rev Lett 78:1396
17. Adamo C, Barone V (1999) J Chem Phys 110:6158
18. Anthony P, Scott LR (1996) J Phys Chem 100:16502
19. Dennington R, Keith T, Millam J (2009) Semichem Inc., Shawnee Mission KS, GaussView, Version 5
20. Reed AE, Curtiss LA, Weinhold F (1988) Chem Rev 88:926
21. Wolinski K, Hilton JF, Pulay P (1990) J Am Chem Soc 112:8251
22. Miertus S, Scrocco E, Tomasi J (1981) Chem Phys 55:117
23. Gejji SP, Bartolotti LJ, Suresh CH, Gadre SR (1997) J Phys Chem A 101:5678
24. Gobre VV, Pinjari RV, Gejji SP (2010) J Phys Chem A 114: 4464
25. Ong W, Kaifer AE (2004) J Org Chem 69:1383
26. Moon K, Kaifer AE (2004) Org Lett 6:185
27. Kim H-J, Jeon WS, Ko YH, Kim K (2002) PNAS 99:5007
28. Bagno A, Rastrelli F, Saielli G (2007) J Org Chem 72:7373
29. Gobre VV, Dixit PH, Khedkar JK, Gejji SP (2011) Comput Theor Chem 976:76
30. Peerannawar SR, Gobre VV, Gejji SP (2012) Comput Theor Chem 983:16